Electromagnetic and Thermal Multi-Physics Design of SPMSM for Wearable Robot

Sung-Woo Hwang, Jun-Woo Chin, Myung-Seop Lim, and Jung-Pyo Hong, *Senior member; IEEE*

Abstract -- **With the rising interest in wearable robot, a lot of researches on the wearable robot is being conducted on aspects of both mechanism and control. On the other hand, although the optimization of the motor has a great effect on the performance of the overall system, research on the motor of the wearable robot remains relatively insufficient. Thus, this paper focuses on a proper design process of the motor of the wearable robot. At first, the surface-mounted permanent magnet synchronous motor (SPMSM) is adopted for its high power density and controllability. Then, the considerations in design of the motor for the wearable robot application are defined and categorized into dimensional, electromagnetic, and thermal requirements. Having taken these into consideration, electromagnetic and thermal multi-physics design for the SPMSM is conducted. For the electromagnetic design, the space harmonic analysis (SHA) is used, and for the thermal analysis, lumped parameter thermal network (LPTN) is used. Following the proposed design process, the optimum SPMSM is designed and manufactured. Finally, experiments of the SPMSM are conducted and the validity of this study is verified.**

Index Terms-- **Electric Motor Design, Space Harmonic Analysis, SPMSM, Lumped Parameter Thermal Network, Wearable Robot**

I. INTRODUCTION

FOR the purpose of rehabilitation in medical areas and power assistance in military and industry areas, wearable robots are gaining increasing attention. Thus, a variety concepts of wearable robots are becoming the subject of intense research recently. In particular wearable robots using electric motors are widely adopted due to better noise and vibration characteristics and smaller size compared to hydraulic and pneumatic actuators [1].

While there are many approaches to the wearable robot in terms of the mechanism and the control, the research on the electric motor remains insufficient [2]. Because the users put on the wearable robot directly on their bodies, the performance of the electric motor as well as the thermal characteristics and its compactness are directly related to user comfort. In order to maximize the users' comfort, it is essential to design an optimum electric motor. Required characteristics of the electric motors for the wearable robot applications are described below.

1) Thin shape with high power density is suitable to minimize the thickness of the joints of the robot
2) Torque ripple and cogging torque of the motor should be minimized to operate the joint motion of the robot smoothly and maximize back-drivability.
3) Thermal characteristics of the motor should be analyzed considering the driving pattern of the joint since the robot come in direct contact with the users' skin.

Few academic papers discuss the design process of permanent magnet (PM) motors to minimize the axial length, torque ripple, and cogging torque, taking into considerations of the thermal characteristics. This paper discusses the design process of the surface-mounted permanent magnet synchronous motor (SPMSM) which is applied to the wearable robot applications [3]. Based on a deep comprehension of the wearable robot application, the requirements for the SPMSM are defined so as to be considered in the design process. Because not only the electromagnetic characteristics but also the thermal characteristics are important for the SPMSM, those two aspects need to be considered simultaneously. For the electromagnetic analysis, the space harmonic analysis (SHA) and the 2-dimensional finite element analysis (2-D FEA) are used [4]. The SHA has acceptable accuracy and is much faster than the 2-D FEA. Thus, it is used in the preliminary design stage. The lumped parameter thermal network (LPTN) which is reasonable in terms of the accuracy and the fast computing time is used for the thermal analysis. Considering these two aspects, an SPMSM that satisfies all the requirements is designed and manufactured. Finally, experiments on the designed SPMSM are carried out in order to verify the validity of this study.

II. REQUIREMENTS

In the design process of an electric motor, features of its application must be considered in order to maximize the performance of the overall system. In this respect, the major requirements for the electric motor of the wearable robot are classified into the three following aspects.

A. Dimensional requirements

For the compactness, the arrangement of the robot system which includes the electric motor, the gear reducer and the lead wires should be efficient. Therefore, the gear reducer is located inside of the rotor of the electric motor and many wires pass through the hollow of the rotor. Consequently, the hollow diameter of the rotor needs to be larger than a certain dimension. Moreover, for the comfort of the user, the electric motor needs to be as small as possible. Thus, there is a limit in terms of the outer diameter of the electric motor. The dimensional requirements for the electric motor for the robot in this paper are organized in Table I. The outer diameter

S. W. Hwang, J. W. Chin, and J. P. Hong are with the Department of Automotive Engineering, Hanyang University, Seoul 04763, Republic of Korea (e-mail: supertramph@hanyang.ac.kr, cjw1254@hanyang.ac.kr, hongjp@hanyang.ac.kr)

M. S. Lim is with the School of Mechanical Engineering, Yeungnam University, Gyeongbuk 38541, Republic of Korea (e-mail: limmang87@yu.ac.kr)

978-1-5386-2477-7/18/$31.00 ©2018 IEEE

should be smaller than 76.0 mm, the inner diameter of the motor which is equal to the hollow diameter should be larger than 36.7 mm and the axial length including the height of the end coils should be shorter than 18.0 mm.

B. Electromagnetic requirements

The purpose of the wearable robot is to assist the user's motion with the torque generated by the electric motors at each joints. There are diverse joints in human body, and the motor designed in this paper is applied to hip and knee joints. Each of joints needs different speed and torque characteristics. Thus, the actuators for those joints are composed of the same motor and different gear reducers. In order to satisfy the target assisting performance of the robot, the electric motor should be able to generate mechanical output. The requirements can be defined with the maximum torque, the base speed and the maximum speed as stated in Table I.

Moreover, the requirements of electrical input must be clarified prior to the initial design process. The electrical requirements which are the DC link voltage and the maximum input current are organized in Table I.

C. Thermal requirements

Because of the exoskeletal structure of the wearable robot, the electric motor is located very close to the user's body. Therefore, the heat generated from the motor is transferred directly to the user's body by conduction through the metal frame and by convection via the ambient. In this respect, the thermal characteristics of the electric motor must be thoroughly investigated in the design process. The thermal requirement is that the end coil temperature must not exceed 35□ when the motor is driven for 30 minutes under the driving pattern of the joint of the wearable robot.

III. SPACE HARMONIC ANALYSIS

In the preliminary design stage, a fast and accurate analysis method is required in order to predict the electromagnetic characteristics of the SPMSM. For the electromagnetic design, there are variety of design parameters that are directly related to the performance of the SPMSM. Thus, it is very important to decide the initial values of the parameters prior to the detail design stage. From this point of view, the space harmonic analysis (SHA) is used for the initial design in this paper.

TABLE I
REQUIREMENTS FOR THE ELECTRIC MOTOR OF THE WEARABLE ROBOT

Contents	Unit	Value
Outer Diameter	mm	< 76.0
Rotor Hollow Diameter	mm	> 36.7
Axial Length	mm	< 18.0
Max. Current	A_{pk}	15.0
DC Link Voltage	V_{DC}	24.0
Max. Torque	Nm	> 0.75
Base Speed	rpm	2800
Max. Speed	rpm	> 4000
Torque Ripple (at rated)	%	< 2.0

In this paper, the SHA as an analytical method was used to determine the pole angle and rotor eccentricity [5]. SHA is based on the following assumptions.

- The PMs have linear demagnetization characteristics and fully magnetized.
- End-effects are neglected.
- The stator and the rotor core have infinite permeability.

In the SHA, the PM is divided into many pieces in order to take into consideration the eccentric shape of PM as shown in Fig. 1. Therefore, different air-gap length is applied to each piece due to the various thicknesses of the PM in the circumferential direction. Accordingly, the same general equation and boundary conditions for the SPMSM without eccentricity can be used with no mathematical error and an exact solution can be obtained. The details of the formula development and equations are described and organized in prior researches as [6] [7]. Air gap flux density distribution in the radial direction and tangential direction obtained using the SHA are compared to the results of the FEA to verify the validity of the method in Fig. 2. The residual induction of the analysis model is 1.0 T, and 10 mm eccentricity is applied. The results show that the flux density distribution using the

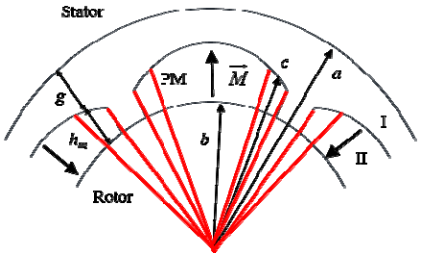

Fig. 1. Geometric configuration of inner rotor type SPMSM

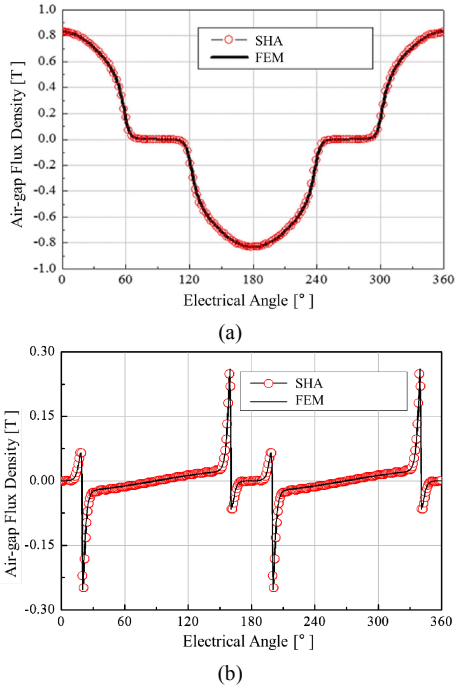

Fig. 2. Comparison of analysis result using SHA and FEA; (a) radial flux density (b) tangential flux density

SHA is almost the same as the result of FEA.

The calculated magnetic field distribution from the Laplace equation is only able to deal with a slot-less stator model. However, the slot opening effect on the magnetic field distribution in the air gap should be considered for the exact prediction of the magnetic field in the slotted model. The air gap flux density of the slotted model can be calculated by multiplying the air gap flux density of the slot-less model by the relative specific permeance [8]. It can be expressed in the following equation.

$$B_{slotless} \times \lambda = B_{slotted} \tag{1}$$

λ is the distribution of the relative specific permeance in the air gap. As relative specific permeance for slot opening is applied to the model, the slot opening effect also can be analyzed. Thus, air gap flux density distribution of the slotted model in the radial and tangential direction can be obtained.

IV. Lumped Parameter Thermal Network

Generally, the thermal FEA and the computational fluid dynamics (CFD) are conducted for the thermal analysis. However, CFD takes much computational resource and time. Therefore, the lumped parameter thermal network (LPTN) is used to analyze the thermal characteristics of the SPMSM in this paper. The LPTN has less accuracy than the thermal FEA with CFD. However, it has advantages in terms of its fast computing time. Furthermore, the LPTN is based on the circuit equations which are expressed by the dimensions and material properties. Thus, it is advantageous to be applied to the parametric design in the preliminary design stage [9].

A. Background

The LPTN is organized based on the equivalence of the electrical system and the thermal system. As organized in Table II, the temperature difference corresponds to the voltage in the electrical system and the heat flow rate, thermal resistance and thermal capacitance correspond to current, electrical resistance and electrical capacitance, respectively. The ways of heat flow through the conduction, the convection and the complex contact states between parts are modeled as resistances in electric circuit based on the assumptions below [10] [11].

1) Radiation is ignored
2) No heat flows in a circumferential direction except for the flow between the stator teeth and windings
3) A single average value represents the temperature of a part ignoring temperature variance in the radial and the axial directions.
4) The thermal capacitance and the heat source are uniformly distributed in each component.

TABLE II
Requirements for the Electric Motor of the Wearable Robot

Contents	Electrical System	Thermal System
Potential	Voltage, V	Temperature difference, ΔT
Flow	Current, I	Heat flow rate, $\dot{Q}$
Resistance	Electrical resistance, R	Thermal resistance, R_t
Capacitance	Electrical capacitance, C	Thermal capacitance, C_t
Equation	$V = IR$	$\Delta T = \dot{Q}R_t$

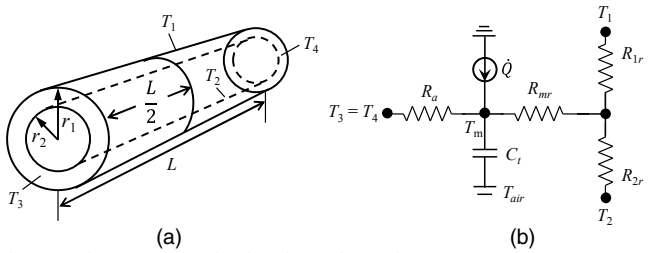

Fig. 3. Element of Conduction thermal transfer

To be distinguished from the former researches on the LPTN, major improved points of the proposed method are explained below.

First, the proposed LPTN considers the heat flow in circumferential direction between stator teeth and windings as the thermal resistance. The proposed LPTN is based on the thermal network which P. H. Mellor proposed [11]. In [11], there is an assumption "There is no circumferential heat flow". However, the losses generated in the stator teeth and windings are different from each other and their temperatures are also different in actual condition. This means that the heat flow between two parts exists and it leads to the necessity of considering the heat flow in circumferential direction.

Secondly, the thermal conductivity of the winding for radial and circumferential direction are considered as the equivalent thermal conductivity of composite material for conductor, insulation and air as proposed by N. Simpson [12]. The proposed LPTN considers the radial, circumferential and axial heat flow of winding. The axial thermal conductivity of winding is almost the same as the thermal conductivity of copper. However, the radial and circumferential thermal conductivity of winding is different from the thermal conductivity of copper because the heat is transmitted through copper, conductor insulation, and air in those directions. The concept of the equivalent thermal conductivity of the winding is cited from the [12] which includes experimental validation for the concept.

B. Thermal conduction

The conduction occurs inside each part of the electric motor such as the rotor, stator yoke, stator tooth, permanent magnets and housing. Due to the shape of the electric motor, particularly for the SPMSM, all these parts can be regarded as a hollow cylindrical shape in (a) of Fig. 3 [13]. Each conduction component is modeled as the electrical circuit shown in (b) of Fig. 3, applying the circumferential periodicity. It consists of the four thermal conduction resistances. The R_a represents the resistance in the axial direction as (2). The R_{1r}, R_{2r}, and R_{mr} represent the resistances of radially outward and inward direction, and compensation, respectively, as stated in (3), (4), and (5).

$$R_a = \frac{L}{6\pi k_a \left(r_1^2 - r_2^2\right)} \tag{2}$$

$$R_{1r} = \frac{1}{2\pi k_r L}\left[1 - 2r_2^2 \ln\left(\frac{r_1}{r_2}\right) \Big/ \left(r_1^2 - r_2^2\right)\right] \quad (3)$$

$$R_{2r} = \frac{1}{2\pi k_r L}\left[2r_1^2 \ln\left(\frac{r_1}{r_2}\right) \Big/ \left(r_1^2 - r_2^2\right) - 1\right] \quad (4)$$

$$R_{mr} = \frac{\left[r_1^2 + r_2^2 - 4r_1^2 r_2^2 \ln\left(\frac{r_1}{r_2}\right) \Big/ \left(r_1^2 - r_2^2\right) - 1\right]}{4\pi\left(r_1^2 - r_2^2\right) k_r L} \quad (5)$$

L is the axial length of the hollow cylinder, k_a, k_r, $r1$, and $r2$ are the axial thermal conductivity, the radial thermal conductivity, the outer and the inner radius, respectively.

C. Thermal convection

For convection in electric motors, the thermal convection resistance, $R_{convection}$ in (6) is related to not only the dimension but also the state of air flow.

$$R_{convection} = \frac{1}{hA} \quad (6)$$

A is the surface area where the convection occurs, and h is the convective heat transfer coefficient in W/(m²·K). The three cases of convection are considered as follow.

1) Frame - ambient
2) Air gap: stator - rotor
3) Endcap air: end cap - stator and rotor

h value varies for each part of the motor: case1) 10~15, case2) 15~20, case3) 100~120. The coefficients are decided by the empirical equations investigated beforehand [14], [15].

D. Heat source and thermal capacitance

The heat sources are the losses of the electric motors such as the copper loss, the iron loss, the eddy current loss in the PMs, and the mechanical loss. The copper loss and the iron loss are calculated by electromagnetic analysis while the eddy current loss in PMs and the mechanical loss are ignored because of their small value. The heat sources are expressed as current sources in the thermal network. The heat sources are separated in detail so as to predict the temperature according to the exact location of the electric motor. For the copper loss, the coil is separated as the end coil and the coil in the slot. $P_{end\ coil}$ and $P_{slot\ coil}$ are the separated copper losses. For the iron loss, it is departmentalized by position of the loss generation as the stator yoke, the stator tooth, the stator tooth tip, and the rotor. The iron losses, P_{yoke}, P_{tooth}, $P_{tooth\ tip}$, and P_{rotor} are shown in Fig. 4.

The thermal capacitance is calculated with the dimensions, the mass density, ρ and the specific heat, c_p by (7).

$$C = \rho c_p \pi\left(r_1^2 - r_2^2\right) L \quad (7)$$

Regarding the aforementioned principles of this study, the LPTN for the SPMSM is modeled in Fig. 4. In addition, the $R_{c,frame}$ defines the thermal contact resistances between the frame and the stator, and the $R_{c,shaft}$ is the thermal contact resistance between the shaft and the rotor. $R_{slot\ liner}$ and $R_{coil\text{-}tooth}$ are the thermal resistance of the slot liner and the resistance between the coil and the stator tooth, respectively.

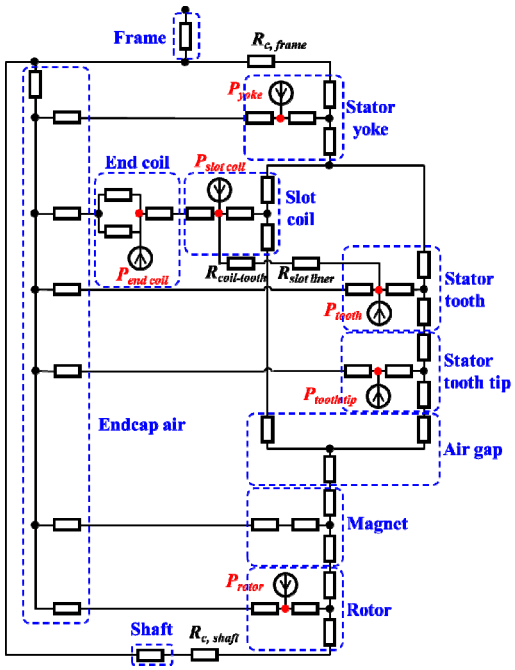

Fig. 4. Lumped parameter thermal network for the SPMSM

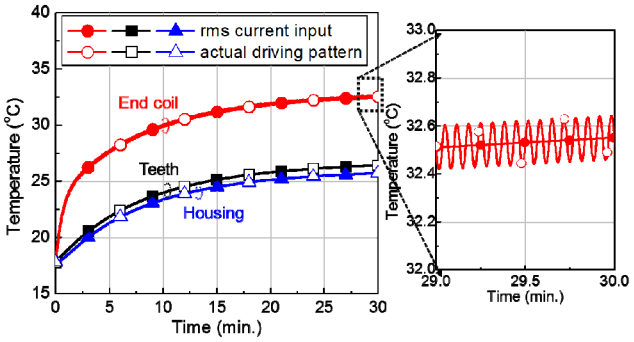

Fig. 5. Comparison of thermal analysis result between the actual driving pattern and RMS current input

E. Consideration of the driving pattern of the motor

Because the driving pattern of the motor affects the thermal characteristics of the motor, it should be considered in thermal analysis. Even though the motor is applied to diverse joints, only driving pattern for the hip joint, which is most severe condition, is considered.

Comparison of thermal analysis results between two different driving patterns is described in Fig. 5. One is the actual driving pattern of hip joint and another is RMS value of current for demand torque of driving pattern. It shows that they have very similar result because the thermal response to the heat generation in the motor is relatively slow while the period of driving pattern based on walking motion is much faster.

Therefore, thermal analysis using RMS value of current for demand torque of driving pattern is effective in terms of

accuracy and also it requires less computation resource and time consumption.

V. DESIGN OPTIMIZATION

A. Preliminary design

First, the number of pole and slot and the winding configuration are decided. Taking into consideration the carrier frequency of the inverter used in the wearable robot system and the target maximum speed of the SPMSM, the number of pole of the SPMSM is limited to 30 in order to generate the sinusoidal input current wave at whole speed range. Then, the following conditions are considered so as to decide upon the winding configuration and the number of pole and slot.

1) High torque: large winding factor
2) Short end coil height: coil pitch should be 1
3) Small cogging torque: large least common multiple of the number of pole and slot
4) Good noise and vibration characteristics

In consideration of the four conditions, the number of pole and slot is decided upon as 14 and 18, respectively.

Next, by using the SHA, the shape of the PM mounted on the rotor core is decided. The shape of the PM is defined with the eccentricity and the pole angle as seen in Fig. 6. It is decided upon by considering the magnitude of the phase back electro-motive force (BEMF), the total harmonic distortion (THD) of the phase BEMF and the cogging torque.

Firstly, the pole angle whose value is represented by pole angle per pole pitch is decided to be set at 0.92 where the magnitude of the phase BEMF is large and the cogging torque is minimized at the same time when the eccentricity is fixed at 0mm as shown in upper graph of Fig. 7. Then, with the pole angle fixed to be 0.92, the eccentricity is decided to be 16mm where the THD of the phase BEMF and the cogging torque is minimized at the same time as shown in the lower graph of Fig. 7.

Prior to the armature design, the required phase BEMF that satisfies the requirements of the mechanical output under the electrical input is calculated.

$$P = T \cdot \omega \le 3 e_{ph} I \tag{8}$$

$$e_{ph} \le V_{ph} = \frac{1}{2} V_{DC} \times \frac{1}{\sqrt{2}} \times Duty\,ratio \times PWM\ factor \tag{9}$$

P represents the power and T, ω, e_{ph}, and I are torque in Nm, rotating speed in rad/s, root mean square (RMS) value of the phase BEMF and RMS line current in A_{rms}, respectively. V_{ph} is the maximum phase voltage that can be fed by the inverter under the DC link voltage V_{DC}. The minimum magnitude of the phase BEMF is calculated with the required mechanical power in (8). The maximum magnitude of the phase BEMF is limited by the phase input voltage in (9). Then, the series turns per phase which makes the phase BEMF have the magnitude between the calculated bounds above is computed by the SHA.

By setting the current density limit as 10 A_{rms}/mm^2 and the slot fill factor to be less than 40%, the diameter of the

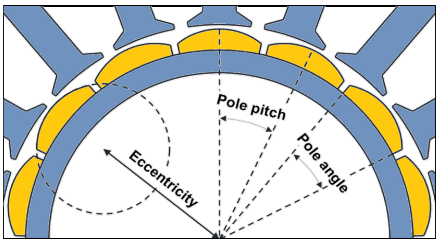

Fig. 6. Eccentricity and pole angle of permanent magnet

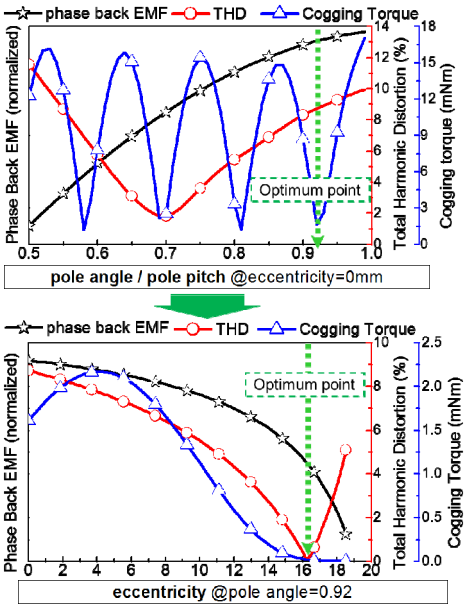

Fig. 7. Decision of the pole angle and the eccentricity using the Space Harmonic Analysis

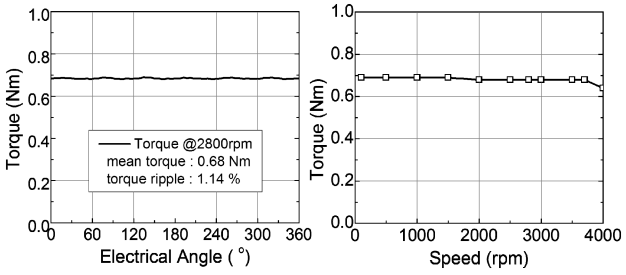

(a) (b)

Fig. 8. Mechanical performance of the initial model; (a) Torque waveform at rated (b) Torque-speed curve

conductor and area of the stator slot are then calculated. Applying the aforementioned dimensional requirements and the area of the stator slot, the shape of the stator core is designed where the reluctance of the magnetic flux path on the stator core is minimized.

As seen in the (a) of Fig. 8, which is obtained by the 2-D FEA, its torque ripple, 1.14%, is small enough for the wearable robot application and its maximum speed is much higher than the requirement. However, the maximum torque of the initial model is not satisfactory for the requirement. Therefore, it is necessary to improve the torque considering the thermal characteristics at the same time.

B. Improvement design

The initial model has a margin of the input voltage which

is directly related to the rotating speed as can be seen in graph (b) of Fig. 8. However, the maximum torque of the motor needs to be improved. Therefore, increasing the number of series turn per phase from 84 turns (initial model) to 90 turns is an appropriate solution to satisfy the requirements in this situation. If the number of turn is increased by making the area of the slot larger, the magnetic saturation of the iron core will become critical and create the possibility of torque decrease. Thus, reducing the diameter of the conductor is more appropriate so as to not increase the magnetic flux density of the iron core. In accordance with their number of winding turn and coil diameter, their stator core shapes which are defined by the teeth and the yoke thickness are optimized by minimizing the reluctance of the stator core, respectively, and it can be seen in the Fig. 9.

The two models whose current densities are higher than the initial model are proposed in Table III. The current densities of model 1 and model 2 are $13A_{rms}/mm^2$ and $15A_{rms}/mm2$ at the maximum current $10.6A_{rms}$, respectively. At the RMS currents for the driving pattern of the joint, their current densities are $4.92A_{rms}/mm^2$ and $5.86A_{rms}/mm^2$, respectively. The maximum torque of the model 1 is 0.76Nm and the model 2 generates 0.78Nm as a maximum. In terms of the maximum torque, both the two proposed models satisfy the requirement, 0.75Nm. The torque improvement is caused by not only an increase in the series turns per phase but also the mitigation of the magnetic saturation of the stator core as can be seen in the Fig. 9 [16].

At this stage, thermal analysis using LPTN is conducted for the three models. As seen in Fig. 10, the end coil temperatures of all three models show their saturating trends when they are driven over 25 minutes. The end coil temperature of the models at 30 minutes are 27.3°C, 32.6°C, and 36.7°C, respectively. The initial model and the model 1 do not exceed the thermal requirement, 35°C but model 2 exceeds such requirements.

C. *Decision on final model*

Both model 1 and model 2 designed under the

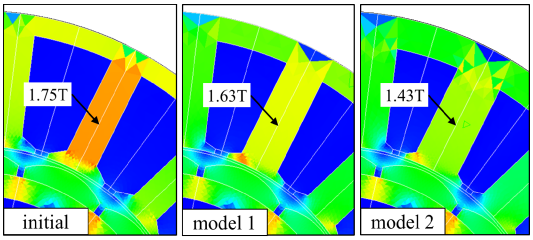

Fig. 9. Comparison of magnetic flux density of stator tooth at rated

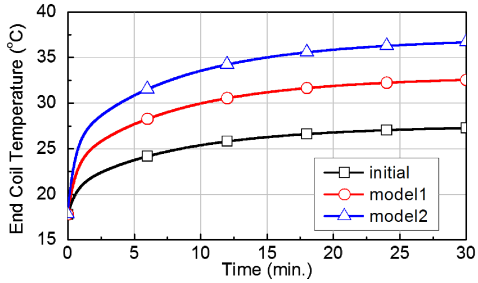

Fig. 10. Trends of end coil temperature under RMS current of driving pattern

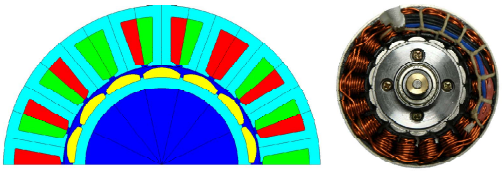

Fig. 11. Final model for the wearable robot; 2-D FEA model (left), manufactured model (right)

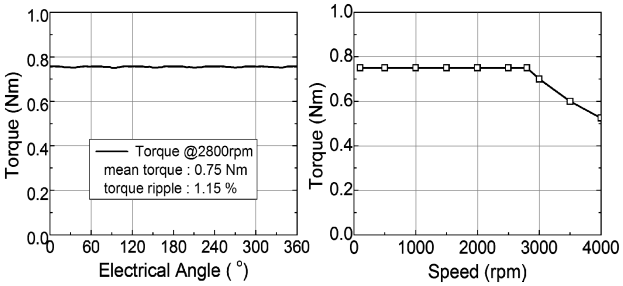

Fig. 12. Final model for the wearable robot; 2-D FEA model (left), manufactured model (right)

requirements of the dimension and the electrical input satisfy the mechanical output requirements. However, in terms of the thermal characteristics, only model 1 meets the requirements. Therefore, model 1 has been selected as the final model. The model for the 2-Dimensional Finite Element Analysis (2-D FEA) and the manufactured motor are shown in Fig. 11. Weight of the machine without the shaft is about 226g. Torque and power density are about 3.32Nm/kg and 0.97kW/kg, respectively. The 2-D FEA result of the final model is shown in Fig. 12. At the base speed, 2800rpm, the mean torque is 0.75Nm and the torque ripple is 1.15%. The Torque-Speed curve in Fig. 12(b) shows that the maximum speed of the model is higher than the requirement.

VI. VERIFICATION

The experimental set shown in Fig. 13 is set to confirm the validity of the simulations used in the design process, such as the SHA, the LPTN, and the 2-D magnetic field FEA. For the torque-speed-current curve comparison in Fig. 14, the measured maximum torque is exact same as the analyzed value. There is a small error between the simulation and measured input line current, and the maximum error is 5.1% at 2800rpm which is deemed acceptable. For the thermal characteristics, the trends of the measured and the analyzed end coil temperature are compared in Fig. 15. The manufactured motor is driven for 30minutes with the driving pattern of the wearable robot. It shows that the error of temperature at 30 minutes is less than 5%, which is accurate enough for the LPTN. The effectiveness of the design process suggested in this paper is demonstrated by comparison with conventional motor in Table IV. Its rotor hollow diameter is much larger than that of the conventional motor and axial length is shorter. It is advantageous for system compactness. Also, DC link voltage is smaller and torque constant is larger than those of conventional motor, so that it is more marginal on controller design.

VII. CONCLUSION

This paper discusses the multi-physics design of SPMSM

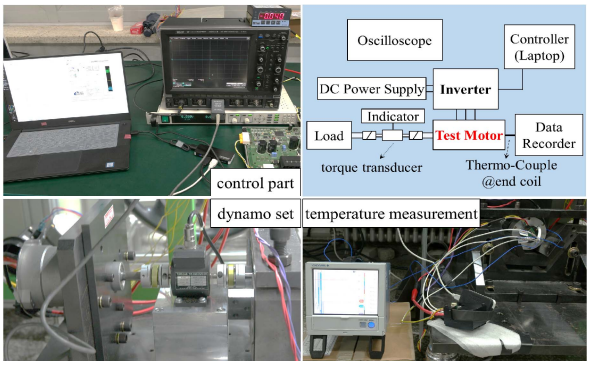

Fig. 13. Experimental set for verification

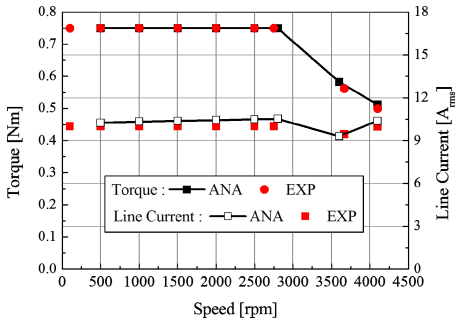

Fig. 14. Comparison of torque-speed-current characteristics

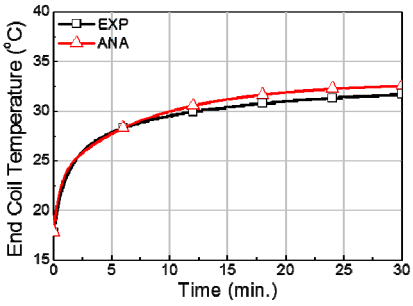

Fig. 15. Comparison of end coil temperature

for wearable robot. Taking the feature of the wearable robot application into account, the dimensional, electromagnetic and thermal requirements are defined. Thus, the electromagnetic and thermal design optimization is carried out. As a result, the final model is proposed and manufactured. Lastly, experiments are conducted to confirm the validity of this study. It is confirmed that the designed motor satisfies requirements. Thus, the effectiveness of using the analysis methods used in this study, which are SHA, LPTN, are demonstrated and their usefulness in multi-physics design can be applied to the other applications.

VIII. REFERENCES

[1] H. Al-Fahaam, S. Davis, and S. Nefti-Meziani, "Power assistive and rehabilitation wearable robot based on pneumatic soft actuators," *International Conference on Methods and Models in Automation and Robotics*, DOI 10/1109/MMAR.2016.7575181, pp.472-477, Sep. 2016

[2] T. Boaventura, and J. Buchli, "*Acceleration-based transparency control framework for wearable robots*," *International Conference on Intelligent robots and Systems*, DOI 10/1109/IROS.2016.7759836, pp5683-5688, Oct. 2016

[3] S. W. Hwang, M. S. Lim, and J. P Hong, "*Hysteresis torque estimation method based on iron-loss analysis for permanent magnet synchronous motor," Transactions on Magnetics,* vol. 52, IA-21, DOI 10/1109/TMAG.2016.2528998, no. 7, pp. 1-4, Jul. 2016.

[4] D. Zarko, D. Ban, and T. A. Lipo, "Analytical Solution for Cogging Torque in Surface Permanent-Magnet Motors Using Conformal Mapping," IEEE Trans. Magn., vol. 44, no. 1, pp. 52–65, Jan. 2008.

[5] L. Wu, and Z. Q. Zhu, "Analytical Modeling of Surface-Mounted PM Machines Accounting for Magnet Shaping and Varied Magnet Property Distribution," IEEE Trans. Magn., vol. 50, no. 7, Art. ID. 8101511, July 2014.

[6] K. C. Lim, J. P. Hong, and G. T. Kim, "The Novel Technique Considering Slot Effect by Equivalent Magnetizing Current," IEEE Trans. Magn., vol. 35, no. 5, pp. 3691-3693, Sept. 1999.

[7] G. H. Kang, and J. P. Hong, "A Novel Design of an Air-Core Type Permanent Magnet Linear Brushless Motor by Space Harmonics Field Analysis," IEEE Trans. Magn., vol. 37, no. 5, pp. 3732-3736, Sept. 2001.

[8] L. Fang, and S. O. Kwon, and J. P. Hong, "Conformal Transformation Technique for Prediction of the Magnetic Field Distribution in an IPM Motor," IEEE Int. Conf. on Electrical Machines and Systems (ICEMS) 2005, vol. 3, pp. 2124-2128, Sept. 2005.

[9] B. H. Lee, K. S. Kim, J. W. Jung, J. P. Hong, and Y. K. Kim, "Temperature Estimation of IPMSM Using Thermal Equivalent Circuit," IEEE Trans. Magn., vol. 48, no. 11, pp. 2949-2952, Nov. 2012.

[10] A. Boglietti, A. Cavagnino, and D. Staton, "Determination of Critical Parameters in Electrical Machine Thermal Models," IEEE Trans. Ind. Appl., vol. 44, no. 4, pp. 1150–1159, Jul./Aug. 2008.

[11] P. H. Mellor, D. Roberts, and D. R. Turner, "Lumped parameter thermal model for electrical machines of TEFC design," IEE Proc., vol. 138, no. 5, pp. 205–218, Sep. 1991.

[12] N. Simpson, R. Wrobel, and P. H. Mellor, "Estimation of Equivalent Thermal Parameters of Impregnated Electrical Windings," IEEE Trans. Ind. Appl., vol. 49, no. 6, pp. 2505–2515, Nov./Dec. 2013.

[13] J. Nerg, M. Rilla, and J. Pyrhönen, "Thermal Analysis of Radial-Flux Electrical Machines With a High Power Density," IEEE Trans. Ind. Electron., vol. 55, no. 10, pp. 3543–3554, Oct. 2008.

[14] Y. A. Cengel, and A. J. Ghajar, Heat and Mass Transfer, Fundamentals and Applications, 5th ed., McGraw-Hill Education, Apr. 2014.

[15] D. A. Howey, P. R. N. Childs, and A. S. Holmes, "Air-Gap Convection in Rotating Electrical Machines," IEEE Trans. Ind. Electron., vol. 59, no. 3, pp. 1367–1375, Mar. 2012.

[16] S. W. Hwang, J. H. Sim, J. P. Hong, J. Lee, and J. Kim, "Torque improvement of wound field synchronous motor for electric vehicle by PM-assist," IEEE Energy Conversion Congress and Exposition (ECCE) 2016, DOI 10/1109/ECCE.2016.7855528, pp. 1-6, Jul. 2016

IX. BIOGRAPHIES

Sung-Woo Hwang received a Bachelor's degree in mechanical engineering from Hanyang University, Seoul, Korea, in 2014. He is currently working toward a Ph.D. in automotive engineering from Hanyang University.

His research interests are electric machine design for automotive and robot applications and numerical analysis of electromagnetics.

Jun-Woo Chin received a Bachelor's degree in mechanical engineering from Hanyang University, Seoul, Korea, in 2014. He is currently working toward a Ph.D. in automotive engineering from Hanyang University.

His research interests are the design of electric machines and thermal analysis of electric motor and generator.

Myung-Seop Lim received the Bachelor's degree in Mechanical Engineering from Hanyang University, Seoul, Korea, in 2012. Also, he received the Master's and Ph.D. degree in Automotive Engineering from the Same University, in 2014 and 2017, respectively. Since 2018, he has been with Yeungnam University, Daegu, Korea, where he is currently an Assistant Professor in Mechanical Engineering.

His research interests include design of electric machines for mechatronics systems such as automotive and robot applications.

Jung-Pyo Hong (SM'97) received Ph.D. degree in electrical engineering from Hanyang University, Korea, in 1995. From 1996 to 2006, he was professor of Changwon National University, Chang-won, Korea. Since 2006 he has been working as a professor in the Hanyang University, Korea.

His research interests are the design of electric machines, optimization and numerical analysis of electromechanics.